Nano Energy 90 (2021) 106504

Contents lists available at ScienceDirect

Nano Energy

journal homepage: www.elsevier.com/locate/nanoen

P2/O3 biphasic Fe/Mn-based layered oxide cathode with ultrahigh capacity and great cyclability for sodium ion batteries

Cong Chen [a,1], Weiyuan Huang [a,1], Yiwei Li [a], Mingjian Zhang [a,*], Kaiqi Nie [b], Jiaou Wang [b], Wenguang Zhao [a], Rui Qi [a], Changjian Zuo [a], Zhibo Li [a], Haocong Yi [a], Feng Pan [a]

[a] School of Advanced Materials, Peking University, Shenzhen Graduate School, Shenzhen 518055, China
[b] Institute of High Energy Physics, Chinese Academy of Sciences, Beijing 100049, China

ARTICLE INFO

Keywords:
Sodium ion batteries
Fe/Mn-based layered oxides
P2/O3 biphasic structure
Ultrahigh capacity
Suppressed phase transition

ABSTRACT

As the representative layered oxide cathode for sodium ion batteries (SIBs) featuring the low cost, P2-type Na-Fe-Mn oxide (NFMO) delivers a high capacity but a limited cycling stability, while O3-type NFMO shows extended cycling lifespan but a lower capacity. Considering the complementarity of two phases in electrochemistry, we successfully designed and fabricated a Fe/Mn-based layered oxide $Na_{0.67}Li_{0.11}Fe_{0.36}Mn_{0.36}Ti_{0.17}O_2$ with a unique P2/O3 biphasic architecture through high-proportion Li/Ti co-substitution. High-proportion Li substitution in transition metal layers triggers the reversible O redox below 4.2 V due to the formation of the special O bonding environment, delivering a highest capacity of 235 mA h g^1 ever reported among all Fe- and Mn-based layered oxide cathodes. Moreover, the unique intersected complex way at the phase boundary significantly suppressed the P2→OP4 phase transition and decreased the lattice mismatch between two phases at high potentials, greatly enhancing the cycling stability. This novel phase complex strategy benefits the design of promising cathode materials with high capacity and long lifespan for SIBs and beyond.

1. Introduction

Lithium-ion batteries (LIBs) are widely applied in consumer electronics and electric vehicles due to their high operating voltage and energy density. However, the increasing demand and limited reserves of lithium cause a rapid rise in the cost. Thus the low-cost sodium ion batteries (SIBs) appear as a promising candidate and set off a research boom due to the earth abundance of sodium [1–6]. Compared with the reported several types of cathode materials for SIBs, like polyanion compounds [7–11], and Prussian analogs [12–14], sodium transition metal layered oxides (Na_xTMO_2) have been extensively studied, due to the high reversible capacity, suitable operating voltage (1.5–4.2 V) and structural simplicity [15,16]. Recently, a series of important advances were made in the Na_xTMO_2 system. Tarascon group reported an O3-type $NaLi_{1/3}Mn_{2/3}O_2$ cathode showing a sustained reversible capacity of 190 mA h g^{-1} and discernible voltage fade on cycling [17]. Li et al. designed a P2-type $Na_{0.7}Mg_{0.2}[Fe_{0.2}Mn_{0.6}\square_{0.2}]O_2$ cathode with the intrinsic vacancies, which implemented reversible oxygen redox in a wide potential range of 1.5–4.5 V [18]. Wang et al. revealed the impact of different Na^+ occupancy sites on the electrochemical performance in a P2-type $Na_{0.67}[Mn_{0.66}Ni_{0.33}]O_2$ cathode [19]. Among these Na_xTMO_2 materials, Fe- and Mn-based layered oxides (NFMO) attract much attention due to the abundant reserves and low cost of Fe and Mn [20,21]. Moreover, the combination of two redox couples of Mn^{3+}/Mn^{4+} and Fe^{3+}/Fe^{4+} makes it attain a relative high energy density (300–500 W h kg^{-1}). With these advantages, NFMO are considered as ideal candidates for the large-scale energy storage devices [4,5,22,23].

In NFMO, the different Na contents lead to different Na^+ crystallographic sites and anionic stacking sequences [24]. Two typical layered structures are P2 and O3 [25]. In P2 structure, Na ions occupy at the triangular prism sites and are facile to diffuse to adjacent sites directly, leading to the fast Na^+ diffusion kinetics, thus the better rate capability and the higher capacity, as compared to O3-type [26–28]. However, P2-type materials undergo the irreversible phase transformation to OP4 phase (also called Z phase) upon repeated Na^+ extraction/insertion, which causes a rapid capacity degradation [29,30]. In O3 structure, Na ions locate at the octahedral sites and Na^+ migration needs to surmount the high energy barriers caused by the intermediate tetrahedral sites,

* Corresponding author.
E-mail address: zhangmj@pkusz.edu.cn (M. Zhang).
[1] These authors contributed equally: Cong Chen and Weiyuan Huang.

https://doi.org/10.1016/j.nanoen.2021.106504
Received 3 June 2021; Received in revised form 6 September 2021; Accepted 6 September 2021
Available online 10 September 2021

leading to the sluggish diffusion kinetics and the low practical capacity [21,31]. Nonetheless, O3-type materials are mostly in Na-sufficient condition and exhibit superior structure stability. In general, the poor cycling stability hinders the development of P2-type materials, while the main bottleneck of O3-type is the low practical capacity [32].

Elemental doping is demonstrated to be an effective way to improve the cycling stability of P2 phase. Ti substitution would not change the phase structure, and the formation of strong Mn—O—Ti—O—Fe bond in the TM layers greatly enhances the structure stability, but at the expense of the capacity decrease due to the inactivity of Ti (the upper panel of Scheme 1) [33–36]. The effects of Li doping greatly depend on the substituted site. When Li ions take at TM sites, the P2 phase is maintained and Li ions can migrate to Na layers as pillars upon charge to enhance the cycling stability [24,37]. When a large amount of Li ions are introduced, P2-type structure tends to transform to O3-type structure with the better structure stability [38–43]. However, Li^+ is also electrochemically inactive, excessive Li substitution would lower the specific capacity [33,44]. In brief, the single elemental substitution can not perfectly solve the concern of the poor stability for P2 phase without sacrificing the capacity.

Considering the complementarity of P2 and O3 phases in electrochemistry and the different effects of Li^+ or Ti^{4+} substitution on tuning the phase structure, we purposely created a P2/O3 biphasic $Na_{0.67}Li_{0.11}Fe_{0.36}Mn_{0.36}Ti_{0.17}O_2$ through high-proportion Li^+ and Ti^{4+} co-substitution in TM layers (the middle panel of Scheme 1). Detailed structural analysis revealed a unique intersected complex way at the phase boundary of two layered phases, which suppressed the phase transformation and enhanced the structural stability. The electrochemical analysis combining with the charge compensation mechanism study confirm the introduction of the reversible O redox during charge/discharge. Therefore, it delivers an ultrahigh capacity of ~ 235 mA h g^{-1} with the great cycling stability (85.4% capacity retention for 100 cycles). Our findings provide guidance to design new cathodes with high energy and long lifespan for SIBs.

2. Results and discussion

2.1. Determination of P2/O3 biphasic structure

To study the impact of Li and Ti substitution on the phase structure, three different strategies were applied in P2-type $Na_{0.67}Fe_{0.5}Mn_{0.5}O_2$ (NFMO), including single Li substitution with 11% Li (denoted as NLFMO), single Ti substitution with 17% Ti (denoted as NFMTO), and Li/Ti co-substitution with 11% Li and 17% Ti (denoted as NLFMTO). The actual elemental compositions were determined by ICP-OES (Table S1). As shown in Fig. 1a-d, XRD patterns were collected to analyze the crystal structures. The Bragg peaks of NFMO can be well indexed to a hexagonal lattice with $P6_3/mmc$ space group, a typical P2 phase (Fig. 1a). The high-resolution transmission electron microscopy (HRTEM) image confirms the layered structure with the (002) interplanar spacing of 5.57 Å (Fig. 1e). When incorporating Li into NFMO, XRD pattern of NLFMO is distinctly different from that of NFMO (Fig. 1b), and can be indexed to a new O3 phase with R-3m space group. This hints that a large amount of Li substitution would induce the phase transition from P2-type structure to O3-type structure [45,46]. Apart from the main O3 phase and the little P2 phase, the impurity Li_2MnO_3 can be observed (marked by the arrow in Fig. 1b), hinting an upper limit value for Li substitution (< 11%). It would lead to an increased Na/TM ratio in the O3 phase than that in the original P2 phase, which may be beneficial to the cycling stability. Different with Li substitution, Ti substitution does not bring significant phase change in NFMTO (Fig. 1c). Similarly, there is also an upper limitation (< 17%) for Ti substitution, indicated by the impurity of $NaFeTiO_4$ (marked by the arrow in Fig. 1c). The structural analysis above demonstrates that, it is difficult to incorporate single element into NFMO by either Li or Ti with a high content. Surprisingly, XRD pattern of NLFMTO can be indexed to P2 phase and O3 phase without any other detectable impurity (Fig. 1d), further confirmed by Raman spectra (Fig. S1). It manifests the synergistic effect of low valent cation Li^+ and high valent cation Ti^{4+}. Rietveld refinements were performed and the results were summarized in Table S2. It is clear to see that, the P2 component of NLFMTO has a much smaller c value than Ti-doped NFMTO, while the O3 component of NLFMTO has a much larger c value than Li-doped NLFMO, which may reflect the larger amount of Ti

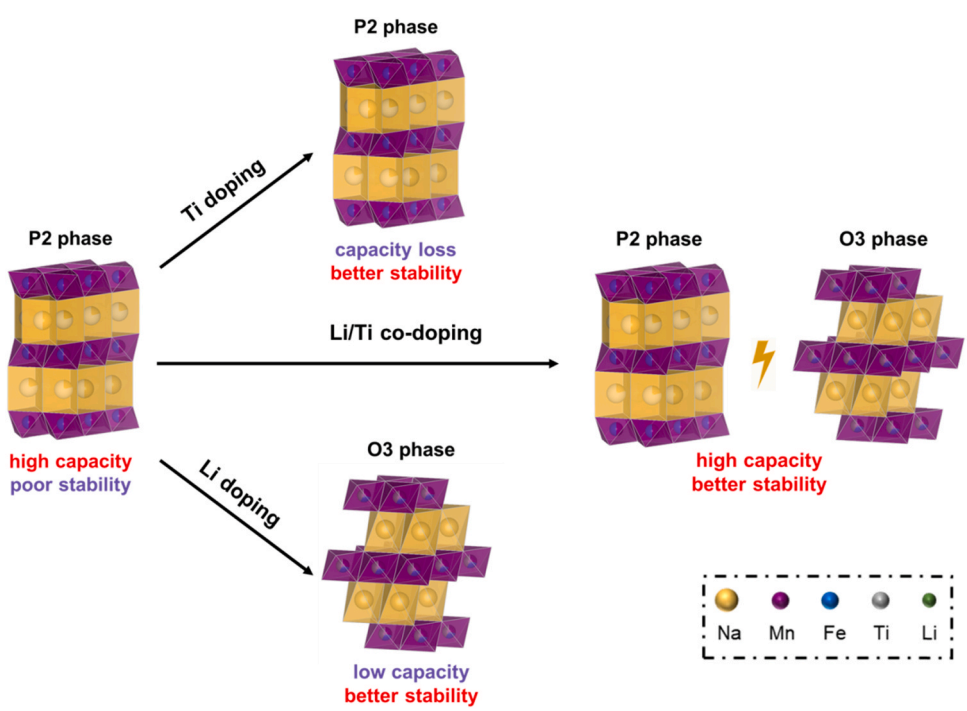

Scheme 1. Schematic illustration of the design of the P2/O3 biphasic structure for sodium Fe/Mn-based layered oxide cathode.

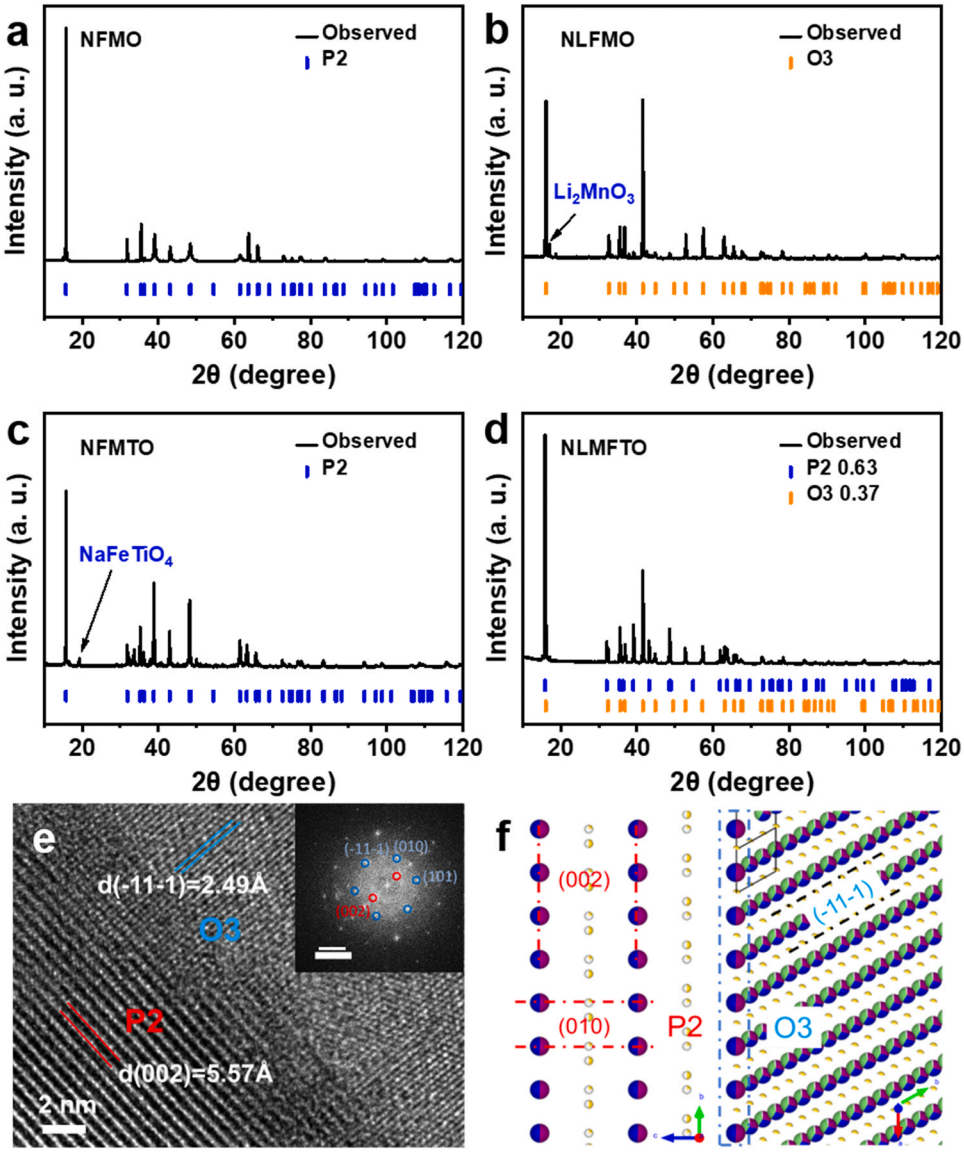

Fig. 1. Determination of the P2/O3 biphasic structure for NLFMTO. XRD patterns and the Rietveld refinement of NFMO (a), NLFMO (b), NFMTO (c), and NLFMTO (d). The arrows in (b) and (c) are used to mark the impurities. (e) HRTEM image at the phase boundary of NLFMTO. Inset is the corresponding FFT map. Red and blue circles are used to mark the reflection spots for P2 and O3 phase, respectively. The scale bar in FFT map is 5 1/nm. (f) Structure illustration to show the unique intersected complex way at the phase boundary between P2 and O3 phase for NLFMTO.

and Li substitution than NFMTO and NLFMO. According to the refinement results, the weight percentages of P2 phase and O3 phase are 63% and 37%, respectively.

To further check the local structure of NLFMTO at the atomic level, HRTEM image (extracted from a small region marked by the yellow dashed square in Fig. S2) and the fast Fourier transform (FFT) map are shown in Fig. 1e. The lattice fringes with the interplanar spacing of 5.57 and 2.49 Å can be ascribed to (002) plane for P2 phase and (− 11–1) plane for O3 phase, respectively. Correspondingly, the reflection spots in the FFT map can be assigned to (002) plane (red cycles) for P2 phase, and (− 11–1), (010), (101) planes (blue cycles) for O3 phase, respectively. The similar complex way can be observed at another phase boundary (Fig. S3), and the corresponding TEM-EDX mapping confirm the uniform elemental distribution of Na, Fe, Mn, and Ti across the phase boundary. Accordingly, the unique complex way between two phases at the phase boundary can be clearly demonstrated in Fig. 1f. (002) plane of P2 phase is intersected with (− 11–1) plane of O3 phase at a certain angle. Such unique intersected complex way is different from the layer-stacking or shoulder-by-shoulder complex way reported before [44, 46–48], and would greatly affect the electrochemical performance, especially the structural stability of P2 phase during cycling (depicted as below). These local observations are consistence with the XRD results above, confirming a P2/O3 biphasic structure in NLFMO.

SEM images were also collected to analyze the influences of elemental substitution on the morphology (Fig. S4). NFMO presents the regular plate-like shape with the homogeneous particle size about 1–2 μm. With Li or Ti single substitution, NFMTO and NLFMO show the irregular shape with the smaller particle size. After Li/Ti co-substitution, NLFMTO exhibits a similar plate-like shape with NFMO, and a larger particle size of 2–4 μm. Corresponding energy dispersive spectroscopy (EDS) mapping indicate that, Fe, Mn, and Ti uniformly distribute in the entire particle.

2.2. Ultrahigh capacity and enhanced cyclability

To study the impact of the different phase structures on the electrochemical performance, NFMO, NLFMO, NFMTO and NLFMTO cathodes were fabricated using the same procedure and tested in sodium half cells. Fig. 2a exhibits the charge-discharge profiles of the four cathodes in the voltage range of 1.5–4.2 V at 0.1 C. NLFMTO shows the highest initial capacity of 235 mA h g^{-1} ever reported among all the Fe- and Mn-based cathodes (Table S3), much higher than that of NFMO, NLFMO and NFMTO (183, 136 and 125 mA h g^{-1}, respectively). Combining with the average voltage 3.0 V, it delivers a high energy density of

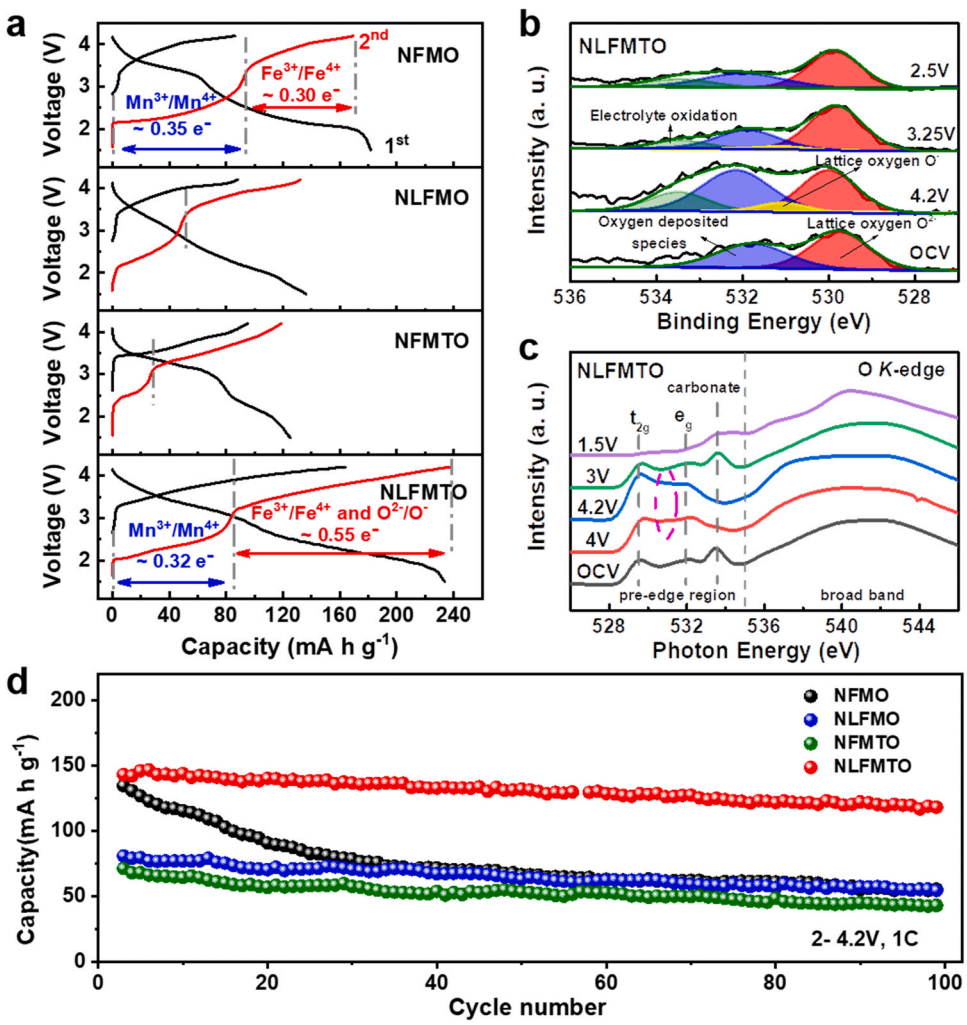

Fig. 2. Improved electrochemical performance. (a) The 1st and 2nd charge-discharge curves of NFMO, NLFMO, NFMTO and NLFMTO at 0.1 C (1 C = 200 mA g^{-1}) in the voltage range of 1.5–4.2 V. (b) O 1*s* XPS spectra for NLFMTO electrodes before cycling (OCV), charged to 3.5, 4.2 V and discharged to 3.25, 2.5, 2.0 and 1.5 V, respectively. (c) O *K*-edge sXAS spectra of NLFMTO before cycling (OCV), charged to 4.0 and 4.2 V, and discharged to 3.0 and 1.5 V. (d) The cycling performance of the four cathodes in the voltage range of 2.0–4.2 V at 1 C.

~ 700 W h kg^{-1}. The low capacity of NLFMO can be ascribed to the increased oxidation state of Mn and the impurity Li_2MnO_3, accompanied with the phase transformation from P2 phase to O3 phase with sluggish Na^+ diffusion kinetics. Similarly, the low capacity of NFMTO can be ascribed to the decrease of Mn and Fe content and the formation of the impurity $NaFeTiO_4$. The theoretical capacity contribution from Mn^{3+}/Mn^{4+} and Fe^{3+}/Fe^{4+} redox couples in NFMO and NLFMTO were estimated in Table S4. One notable point is that, there is only Fe^{3+}/Fe^{4+} redox couple during the 1st charge since Mn is + 4 in pristine NFMO and NLFMTO. The practical 1st charge capacity for NLFMTO is around 160 mA h g^{-1}, much larger than the estimated capacity from Fe^{3+}/Fe^{4+} redox couple (100.1 mA h g^{-1}), hinting the oxygen redox couple involving at high potentials.

To explore the charge compensation mechanism for the ultrahigh capacity, the charge branch in the 2nd cycle was carefully examined. As for four electrodes, the 2nd charge branch can be generally divided to two parts (marked by the dashed vertical lines in Fig. 2a). The part below 3 V comes from the Mn^{3+}/Mn^{4+} redox couple, while the part above 3 V comes from Fe^{3+}/Fe^{4+} redox couple [29,38]. According to the separate capacity contribution from each part, Mn^{3+}/Mn^{4+} couple contributes 0.35 electrons, and Fe^{3+}/Fe^{4+} couple contributes 0.30 electrons for NFMO. Surprisingly for NLFMTO, the part above 3 V corresponds to 0.55 electrons, which is beyond for the theoretical capacity contribution from Fe^{3+}/Fe^{4+} redox couple based on the chemical formula (0.36 electrons). Considering the electrochemically inactivity of Li^+ and Ti^{4+}, the excessive capacity contribution can only be assigned to O^{2-}/O^- redox at high potentials. The reversible O redox may be triggered by the special bonding environment of oxygen with Na^+/Li^+ in both TM layers and Na layers, similar to what has been frequently observed and extensively discussed in the Li- and Mn-rich layered cathode for LIBs [24,49]. It should be related with a large amount of Li substitution (11%) in the lattice. The corresponding dQ/dV curves and the CV curves during the initial several cycles are shown in Figs. S5 and S6, consistent with the analysis above. The CV curve of NLTMTO is a combination of those of NFMO and NLFMO, further reflecting a biphasic complex structure.

To detect the possible O^{2-}/O^- redox occurred above 3 V, the O 1*s* XPS spectra were collected on NLFMTO electrodes at different charge/discharge states (Fig. 2b). Two peaks at around 533.4 and 532.0 eV correspond to the C—O and C═O bonds from electrolyte oxidation and oxygen deposited species, respectively [50–53]. Notably, the signal of lattice O^- (the orange peak) is observed at 531.1 eV when charged to 4.2 V, and diminishes when discharged to 3.25 V, then disappears after discharged to 2.5 V, indicating lattice O^{2-} anions are reversibly participated in the electrochemical redox reaction during the charge/discharge process. In contrast, there is no O^- anionic peak during the whole charge/discharge process of NFMO (Fig. S7), revealing the electrochemical inert of the lattice O^{2-} anion in NFMO. O *K*-edge soft X-ray absorption spectra (sXAS) further confirm the oxygen redox reaction in NLFMTO. As shown in Fig. 2c, a shoulder feature appears at 531 eV (marked by a dashed ellipse) related to the oxygen redox (lattice O^-) when charged to 4.0 and 4.2 V [54–57], and disappears when discharged below 3.0 V. In addition, two peaks at 529.5 and 532 eV corresponding to the electron transition from O 1*s* state to TM t_{2g} and e_g

state, respectively, show negligible change, hinting the preservation of TMO_6 octahedra. The carbonate species at 533.6 eV disappears when charged to 4.0 and 4.2 V, and re-appears when discharged to 3.0 and 1.5 V, which should be related with the surface side reaction between the cathode and the electrolyte. In addition, Mn *L*-edge sXAS spectra are deposited in Fig. S8a, which further confirms Mn^{3+}/Mn^{4+} redox couple below 3 V, consistent with the deduction above. To validate the reversibility of O redox, *in situ* differential electrochemical mass spectroscopy (DEMS) test was performed during the first cycle of NLFMTO (Fig. S9). There is no significant O_2 release, confirming the good reversibility of O redox. A small amount of CO_2 starts releasing above 3.5 V and gradually reaches the peak at 4.2 V, which may come from the

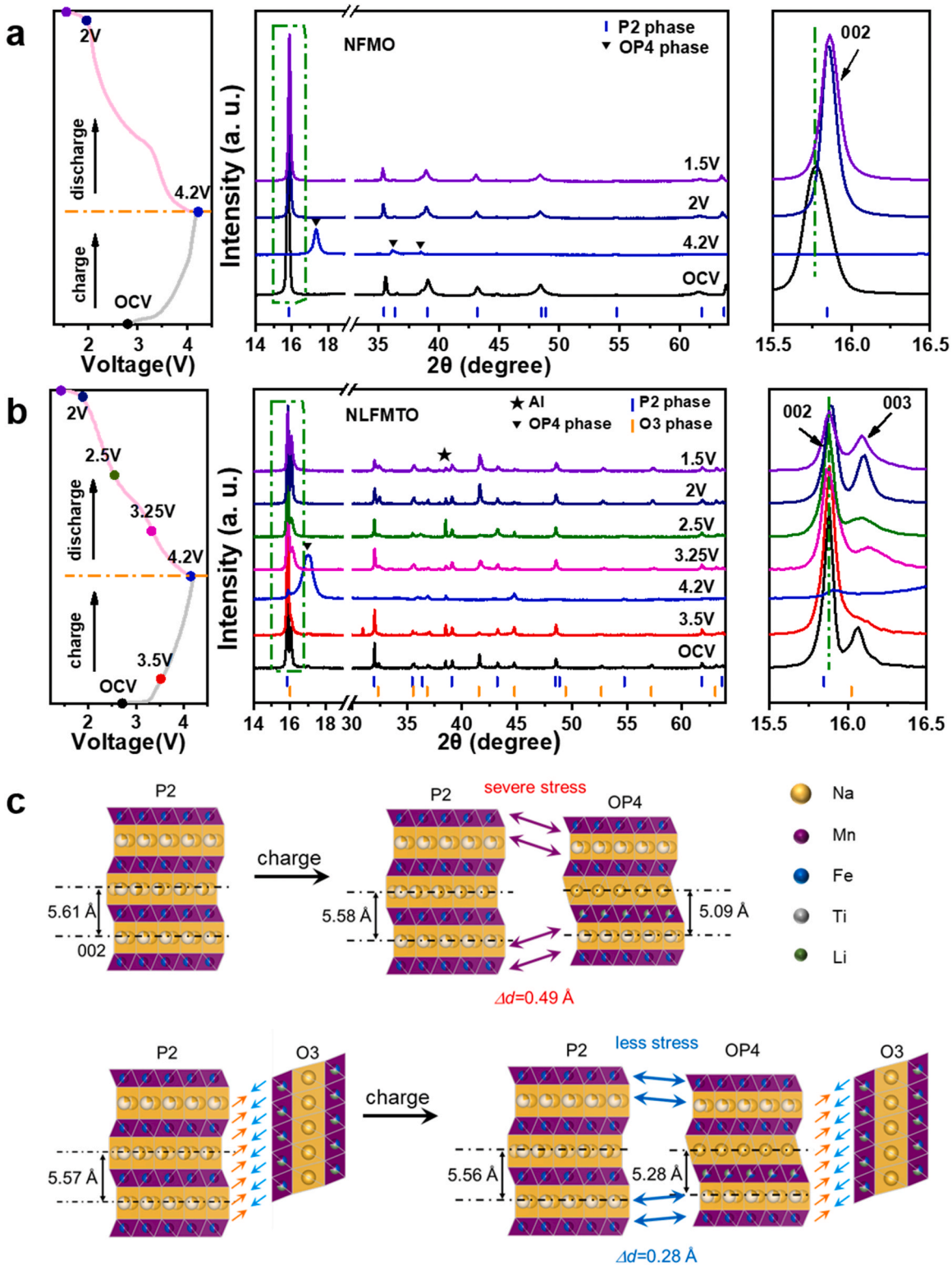

Fig. 3. Phase transformation during the 1st cycle. The 1st charge/discharge curves with the selected voltage points (marked by the dots) as well as the corresponding XRD patterns for NFMO (a) and NLFMTO (b) to track the phase transformation. The regions of 15.5–16.5° were enlarged on the right panels. (c) Schematic view of the structure changes during the charge of NFMO and NLFMTO.

side reaction of electrolyte decomposition at the particle surface.

The cycling performance was comprehensively evaluated. As shown in Fig. 2d, when cycled in 2.0–4.2 V at 1 C (1 C = 200 mA g^{-1}), NLFMTO shows the highest capacity retention of 85.4% after 100 cycles, much better than NFMO, NLFMO and NFMTO (40.9%, 71%, and 63.4%, respectively). Even after 300 cycles, it can still retain a capacity above 100 mA h g^{-1}, in contrast to NFMO (< 50 mA h g^{-1}, Fig. S10). The average voltage was plotted as a function of the cycle number (Fig. S11), indicating the best voltage retention for NLFMTO. The corresponding charge-discharge profiles are presented in Fig. S12. The cycling results in the voltage range of 1.5–4.2 V further confirm the best stability for NLFMTO (Fig. S13). The relatively poor cycling stability in 1.5–4.2 V than that in 2.0–4.2 V can be understood, since the charge/discharge below 2 V would involve more Mn^{3+} content, which may induce Jahn-Teller distortion and structure degradation. The rate performance of NFMO and NLFMTO are displayed in Fig. S14. NLFMTO retains a high capacity of 172 mA h g^{-1} at 1 C, while NFMO only retains 140 mA h g^{-1}.

2.3. Suppressed P2→OP4 phase transformation

To explore the mechanism of the enhanced cycling stability by the P2/O3 biphasic structure, XRD patterns at selected voltage points during the 1st charge/discharge are collected to analyze the phase transformation of NFMO and NLFMTO (Fig. 3a–b). When charged to 4.2 V, P2-type NFMO completely transforms to an OP4 phase (marked by the inverted triangles in Fig. 3a). When discharged to 2.0 and 1.5 V, OP4 phase returns to P2 phase. The (002) peak does not go back to the original position (the right panel of Fig. 3a), hinting the poor reversibility. Such P2-OP4 phase transformation coincides with the previous reports [20]. Accompanying with the phase transformation, the interlayer spacing of (002) peak undergoes a dramatic change from 5.61 Å (OCV), to 5.09 Å (4.2 V), then to 5.58 Å (2.0 and 1.5 V). The big lattice change would cause severe lattice mismatch and distortion at the phase boundary during the phase transformation, which should be the structural origin for the poor cycling stability of NFMO. As shown in Fig. 3b, NLFMTO with a P2/O3 biphasic structure also transforms to OP4 phase when charged to 4.2 V. Nonetheless, the main peak of OP4 phase (marked by the inverted triangle) corresponds to a layer spacing of 5.28 Å, much larger than that of NFMO (5.09 Å). In addition, there is still a small (002) peak left when charged to 4.2 V (the right panel of Fig. 3b), hinting the preservation of a small amount of P2 phase. These two observations indicate that, the P2-OP4 phase transformation is partially suppressed and the lattice mismatch between two phases is greatly decreased in such a P2/O3 biphasic structure. Moreover, the (002) peak nearly goes back to the original position after discharged to 1.5 V (marked by the dashed vertical line in the right panel of Fig. 3b), hinting the excellent reversibility of phase transformation. In the meanwhile, the main peak (003) of O3 phase gradually weakens and disappears when charged to 3.5 V and 4.2 V, and restores to the original position and intensity when discharged to 1.5 V. It indicates that, a reversible phase transformation for O3 phase concurrently proceeds with that of P2 phase. These two kinds of phase transformations may synergistically interact with each other, and contribute to the enhanced cycling stability.

When combining with the unique intersected complex way between P2 and O3 phase revealed above, we propose a mechanism to explain the interplay of two phases for the excellent cycling stability. As shown in the upper panel of Fig. 3c, for P2-type NTMO, the big lattice mismatch between P2 and OP4 phase (Δd = 0.49 Å) leads to the severe stress, which results in the structure collapse and the destruction of the particle integrity, and thus the poor cycling stability. Differently, NLFMTO has a unique P2/O3 biphasic structure, wherein the edge of P2 phase is pinned by the TM layers of the O3 phase. By comparing the structure of P2 and OP4 phase, the P2-OP4 phase transformation must undergo an interlayer sliding between neighboring TM layers in P2 phase (illustrated in Fig. S15). Once the layered structure of P2 phase is pinned by O3 phase, the interlayer sliding is greatly suppressed upon charge, thereby leading to the suppressed phase transformation. Finally, less OP4 phase is formed with much smaller lattice mismatch (Δd = 0.28 Å). Therefore, the reversibility of the phase transformation is greatly enhanced, delivering the better cycling stability for NLFMTO. Different from the previous reports about the P2/O3 biphasic cathodes [43,58–60], the relationship between the biphasic complex way and the enhanced electrochemical performance is clearly illustrated here.

2.4. Structure stability upon repeated cycles

To further investigate the structure stability after long-term cycling, XRD patterns of NFMO and NLFMTO electrodes after 1 cycle and 100 cycles are collected. As shown in Fig. 4a, the main peak (002) of P2-type NFMO obviously shifts to higher angle after 100 cycles as compared with that after 1 cycle (the dashed line in the right panel of Fig. 4a), indicating the big shrinkage of the corresponding interlayer spacing. In contrast, the (002) peak for P2 phase in NLFMTO shows a much smaller shift, indicating the suppressed structural degradation (the dashed line in the right panel of Fig. 4c). While the main peak (003) of O3 phase presents a large shift to higher angle. It hints that, O3 phase may undergo relatively large structural change after long-term cycling. Furthermore, HRTEM images are taken to examine the local structure change of NFMO and NLFMTO cathodes after 100 cycles (Fig. 4b–d). As for NFMO (Fig. 4b), the interlayer spacing is 5.46 Å, much smaller than the initial value 5.61 Å, which is consistent with the XRD results (Fig. 4a). The dispersed reflection spots in FFT map also demonstrate that, the long-term cycling leads to lots of structure disordering in NFMO. Most importantly, massive intragranular micro-cracks can be observed, which should be originated from the accumulated intragranular strain due to the large lattice mismatch between P2 phase and OP4 phase mentioned above. As for NLFMTO (Fig. 4d), the clear lattice fringes confirm a well layered structure with an interlayer spacing of 5.56 Å, close to the initial value 5.57 Å, and consistent with the XRD results (Fig. 4c). The spots in the FFT map are still acute, indicating that the structure is still in highly order. No micro-cracks can be observed, showing the good mechanistic integrity of primary grains for NLFMTO.

Mn dissolution is always another important factor to result into the structure degradation of Mn-based layered oxides during cycling [61–64]. To quantitatively investigate Mn dissolution here, X-ray fluorescence (XRF) test is carried out to quantify the Mn/Fe ratio in the cathode electrodes after 100 cycles (Table S5 and Fig. 4e). As we can see, NLFMTO shows a highest Mn/Fe molar ratio of 90.5%, indicating a little Mn dissolution. By comparison, NFMO shows a much lower Mn/Fe ratio of 76.9%, suggests a severe Mn dissolution in NFMO, which should be related to lots of microcracks observed above. The more severe Mn dissolution in NLFMO and NFMTO may be related to the formation of the impurity.

Combined all these experimental results together, the structural change after long-term cycling can be schematically illustrated in Fig. 4f. NFMO undergoes the serious lattice mismatch during the P2-OP4 phase transformation at high potentials of repeated cycles, which causes lots of micro-cracks in the primary particles, increasing the contact areas with the electrolyte, therefore leading to more side reactions and Mn dissolution. In NLFMTO, the phase transformation and the lattice mismatch for P2 phase are greatly suppressed by the unique intersected complex way with the O3 phase, enhancing the reversibility of the structure change during cycling, and inhibiting the formation of micro-cracks and Mn dissolution.

3. Conclusions

In summary, a P2/O3 biphasic compound $Na_{0.7}Li_{0.11}Fe_{0.36}Mn_{0.36}Ti_{0.17}O_2$ was designed and synthesized by a Li/Ti co-substitution strategy. High proportion Li substitution in TM layers

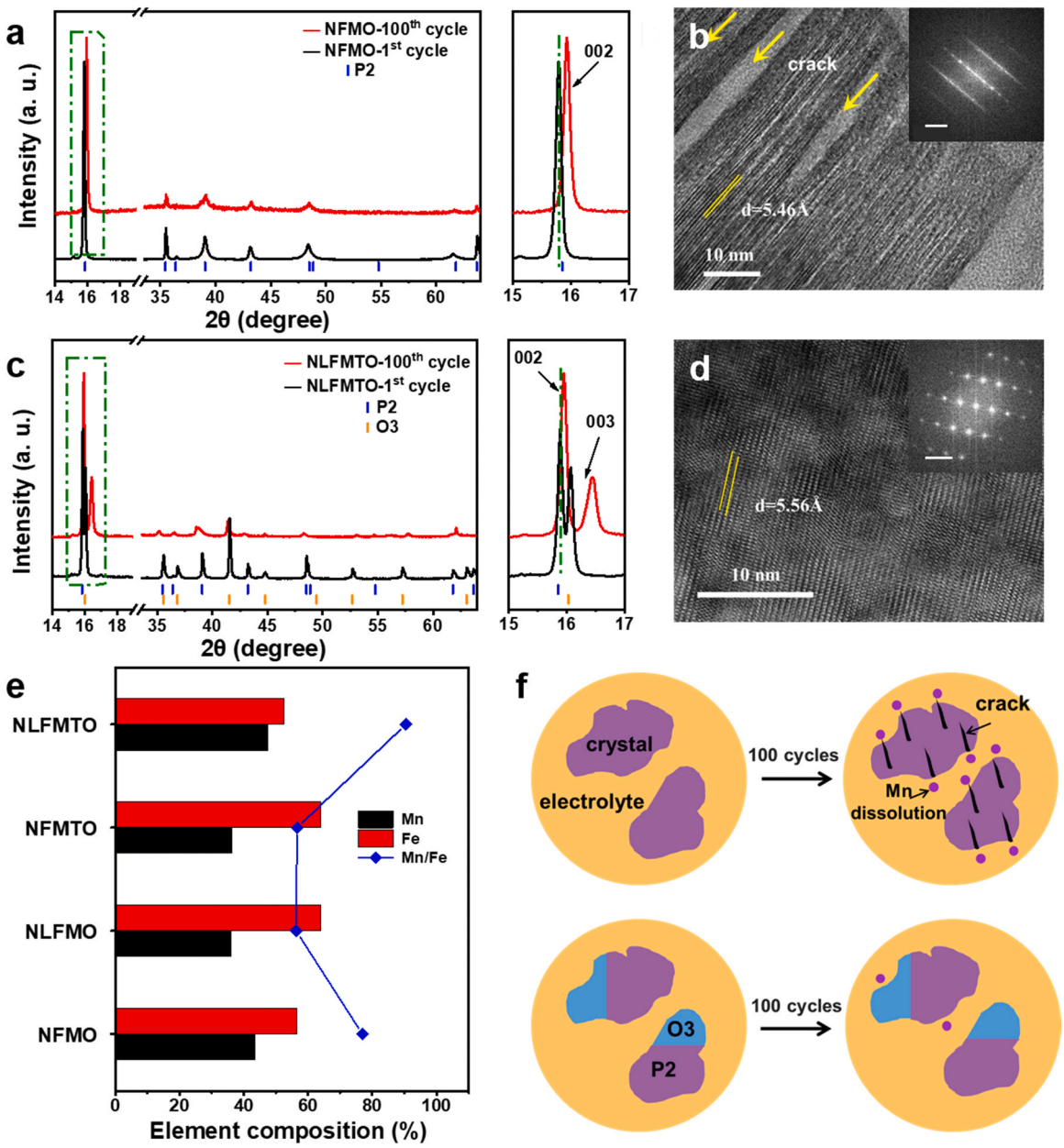

Fig. 4. The structure stability after long-term cycling. XRD patterns of NFMO electrodes (a) and NLFMTO electrodes (c) after 1 cycle and 100 cycles in 1.5–4.2 V. The main peaks marked by the dashed rectangles were enlarged on the right panel to examine the subtle structure changes. HRTEM images for NFMO electrode (b) and NLFMTO electrode (d) after 100 cycles to check the local structure change. The insets are the corresponding FFT maps with the scale bars as 5 1/nm. (e) The Fe/Mn relative contents and the deduced Mn/Fe ratio detected by XRF test for NFMO, NLFMO, NFMTO and NLFMTO after 100 cycles. (f) Schematic illustration of the structural changes for P2-type NFMO and P2/O3 biphasic NLFMTO after long-term cycling.

induced the formation of the unique O bonding environments similar with those in Li-rich Mn-based layered oxides, which triggers the reversible anionic redox activity. Thus an ultrahigh capacity (~ 235 mA h g^{-1}) is achieved among all Fe- and Mn-based layered oxides ever reported for SIBs. In the meanwhile, the phase transformation from P2 phase to OP4 phase at high potentials is partially suppressed and the lattice mismatch between two phases is greatly decreased by the unique intersected complex way between P2 and O3 phase. Therefore, the lattice mismatch and distortion are mitigated to a great extent, and inhibit the formation of micro-cracks and Mn dissolution. Eventually, a great cycling reversibility (85.4% for 100 cycles) can be achieved simultaneously. This work opens a new opportunity to design new high performance cathode materials for SIBs through the complex structure chemistry.

Supporting information

Additional figures and tables about Raman spectra, morphology characterization, elemental distribution, XPS analysis, soft X-ray absorption spectra, *in situ* DEMS data, electrochemical performance, ICP-OES results, Rietveld refinement results, and detailed electrochemical performance comparison table of the reported sodium Fe/Mn-based layered oxides, along with experimental details and instrumental information.

CRediT authorship contribution statement

Cong Chen: Conceptualization, Investigation, Visualization, Methodology, Formal analysis, Writing – original draft. **Weiyuan Huang:**

Conceptualization, Investigation, Visualization, Methodology, Formal analysis. **Yiwei Li:** Investigation, Formal analysis. **Mingjian Zhang*:** Conceptualization, Investigation, Visualization, Formal analysis, Writing – review & editing. **Kaiqi Nie:** Resources. **Jiaou Wang:** Resources. **Wenguang Zhao:** Investigation. **Rui Qi:** Investigation. **Changjian Zuo:** Investigation. **Zhibo Li:** Investigation. **Haocong Yi:** Investigation. **Feng Pan:** Supervision, Project administration, Funding acquisition.

Declaration of Competing Interest

The authors declare that they have no known competing financial interests or personal relationships that could have appeared to influence the work reported in this paper.

Acknowledgments

C. Chen and W. Huang contributed equally to this work. The authors acknowledge support from the National Key R&D Program of China (2016YFB0700600), the Shenzhen Science and Technology Research Grant (No. JCYJ20200109140416788), the Chemistry and Chemical Engineering Guangdong Laboratory (Grant no. 1922018), and the National Key R&D Program of China (2020YFB0704500).

Appendix A. Supplementary material

Supplementary data associated with this article can be found in the online version at doi:10.1016/j.nanoen.2021.106504.

References

[1] R. Berthelot, D. Carlier, C. Delmas, Electrochemical investigation of the P2–Na_xCoO_2 phase diagram, Nat. Mater. 10 (2011) 74–80.
[2] N. Yabuuchi, K. Kubota, M. Dahbi, S. Komaba, Research development on sodium-ion batteries, Chem. Rev. 114 (2014) 11636–11682.
[3] J.Y. Hwang, S.T. Myung, Y.K. Sun, Sodium-ion batteries: present and future, Chem. Soc. Rev. 46 (2017) 3529–3614.
[4] M. Chen, Q. Liu, S.W. Wang, E. Wang, X. Guo, S.L. Chou, High-abundance and low-cost metal-based cathode materials for sodium-ion batteries: problems, progress, and key technologies, Adv. Energy Mater. 9 (2019), 1803609.
[5] X. Wang, S. Roy, Q. Shi, Y. Li, Y. Zhao, J. Zhang, Progress in and application prospects of advanced and cost-effective iron (Fe)-based cathode materials for sodium-ion batteries, J. Mater. Chem. A 9 (2021) 1938–1969.
[6] F.X. Ding, F. Gao, X.H. Rong, K. Yang, Y.X. Lu, Y.-S. Hu, Mixed-phase $Na_{0.65}Li_{0.13}Mg_{0.13}Ti_{0.74}O_2$ as a high-performance Na-ion battery layered anode, Acta Phys. -Chim. Sin. 36 (2020), 1904022.
[7] W.X. Song, X.B. Ji, Z.P. Wu, Y.R. Zhu, Y.P. Yao, K. Huangfu, Q.Y. Chen, C.E. Banks, Na_2FePO_4F cathode utilized in hybrid-ion batteries: a mechanistic exploration of ion migration and diffusion capability, J. Mater. Chem. A 2 (2014) 2571.
[8] Q. Ni, Y. Bai, F. Wu, C. Wu, Polyanion-type electrode materials for sodium-ion batteries, Adv. Sci. 4 (2017), 1600275.
[9] H. Kim, I. Park, D.H. Seo, S. Lee, S.W. Kim, W.J. Kwon, Y.U. Park, C.S. Kim, S. Jeon, K. Kang, New iron-based mixed-polyanion cathodes for lithium and sodium rechargeable batteries: combined first principles calculations and experimental study, J. Am. Chem. Soc. 134 (2012) 10369–10372.
[10] Z.L. Jian, W.Z. Han, X. Lu, H.X. Yang, Y.S. Hu, J. Zhou, Z.B. Zhou, J.Q. Li, W. Chen, D.F. Chen, L.Q. Chen, Superior electrochemical performance and storage mechanism of $Na_3V_2(PO_4)_3$ cathode for room-temperature sodium-ion batteries, Adv. Energy Mater. 3 (2013) 156–160.
[11] W.L. Pan, W.H. Guan, Y.Z. Jiang, Research advances in polyanion-type cathodes for sodium-ion batteries, Acta Phys. -Chim. Sin. 36 (2020), 1905017.
[12] L. Wang, Y.H. Lu, J. Liu, M.W. Xu, J.G. Cheng, D.W. Zhang, J.B. Goodenough, A superior low-cost cathode for a Na-ion battery, Angew. Chem. Int. Ed. Engl. 52 (2013) 1964–1967.
[13] Y. You, X.L. Wu, Y.X. Yin, Y.G. Guo, High-quality Prussian blue crystals as superior cathode materials for room-temperature sodium-ion batteries, Energy Environ. Sci. 7 (2014) 1643–1647.
[14] Y.H. Lu, L. Wang, J.G. Cheng, J.B. Goodenough, Prussian blue: a new framework of electrode materials for sodium batteries, Chem. Commun. 48 (2012) 6544–6546.
[15] Y. Xiao, N.M. Abbasi, Y.F. Zhu, S. Li, S.J. Tan, W. Ling, L. Peng, T.Q. Yang, L. D. Wang, X.D. Guo, Y.X. Yin, H. Zhang, Y.G. Guo, Layered oxide cathodes promoted by structure modulation technology for sodium-ion batteries, Adv. Funct. Mater. 30 (2020), 2001334.
[16] M.H. Han, E. Gonzalo, G. Singh, T. Rojo, A comprehensive review of sodium layered oxides: powerful cathodes for Na-ion batteries, Energy Environ. Sci. 8 (2015) 81–102.
[17] Q. Wang, S. Mariyappan, G. Rousse, A.V. Morozov, B. Porcheron, R. Dedryvere, J. P. Wu, W.L. Yang, L.T. Zhang, M. Chakir, M. Avdeev, M. Deschamps, Y.S. Yu, J. Cabana, M.L. Doublet, A.M. Abakumov, J.M. Tarascon, Unlocking anionic redox activity in O3-type sodium 3d layered oxides via Li substitution, Nat. Mater. 20 (2021) 353–361.
[18] X.L. Li, T. Wang, Y.F. Yuan, X.Y. Yue, Q.C. Wang, J.Y. Wang, J. Zhong, R.Q. Lin, Y. Yao, X.J. Wu, Z.W. Fu, Y.Y. Xia, X.Q. Yang, T.C. Liu, K. Amine, Z. Shadike, Y. N. Zhou, J. Lu, Whole-voltage-range oxygen redox in P2-layered cathode materials for sodium-ion batteries, Adv. Mater. 33 (2021), 2008194.
[19] Q.C. Wang, Z. Shadike, X.L. Li, J. Bao, Q.Q. Qiu, E.Y. Hu, S.M. Bak, X.H. Xiao, L. Ma, X.J. Wu, X.Q. Yang, Y.N. Zhou, Tuning sodium occupancy sites in P2-layered cathode material for enhancing electrochemical performance, Adv. Energy Mater. 11 (2021), 2003455.
[20] N. Yabuuchi, M. Kajiyama, J. Iwatate, H. Nishikawa, S. Hitomi, R. Okuyama, R. Usui, Y. Yamada, S. Komaba, P2-type $Na_x[Fe_{1/2}Mn_{1/2}]O_2$ made from earth-abundant elements for rechargeable Na batteries, Nat. Mater. 11 (2012) 512–517.
[21] N.A. Katcho, J. Carrasco, D. Saurel, E. Gonzalo, M. Han, F. Aguesse, T. Rojo, Origins of bistability and Na ion mobility difference in P2- and O_3-$Na_{2/3}Fe_{2/3}Mn_{1/3}O_2$ cathode polymorphs, Adv. Energy Mater. 7 (2017), 1601477.
[22] Y. Fang, Z. Chen, L. Xiao, X. Ai, Y. Cao, H. Yang, Recent progress in iron-based electrode materials for grid-scale sodium-ion batteries, Small 14 (2018), 1703116.
[23] H.L. Pan, Y.S. Hu, L.Q. Chen, Room-temperature stationary sodium-ion batteries for large-scale electric energy storage, Energy Environ. Sci. 6 (2013) 2338.
[24] L. Yang, X. Li, J. Liu, S. Xiong, X. Ma, P. Liu, J. Bai, W. Xu, Y. Tang, Y.Y. Hu, M. Liu, H. Chen, Lithium-doping stabilized high-performance P2-$Na_{0.66}Li_{0.18}Fe_{0.12}Mn_{0.7}O_2$ cathode for sodium ion batteries, J. Am. Chem. Soc. 141 (2019) 6680–6689.
[25] C. Delmas, C. Fouassier, P. Hagenmuller, Structural classification and properties of the layered oxides, Physica B+C 99 (1980) 81–85.
[26] S.P. Ong, V.L. Chevrier, G. Hautier, A. Jain, C. Moore, S. Kim, X. Ma, G. Ceder, Voltage, stability and diffusion barrier differences between sodium-ion and lithium-ion intercalation materials, Energy Environ. Sci. 4 (2011) 3680.
[27] D.H. Lee, J. Xu, Y.S. Meng, An advanced cathode for Na-ion batteries with high rate and excellent structural stability, Phys. Chem. Chem. Phys. 15 (2013) 3304–3312.
[28] Y. Mo, S.P. Ong, G. Ceder, Insights into diffusion mechanisms in P2 layered oxide materials by first-principles calculations, Chem. Mater. 26 (2014) 5208–5214.
[29] B.M. de Boisse, D. Carlier, M. Guignard, L. Bourgeois, C. Delmas, P2-$Na_xMn_{1/2}Fe_{1/2}O_2$ phase used as positive electrode in Na batteries: structural changes induced by the electrochemical (de)intercalation process, Inorg. Chem. 53 (2014) 11197–11205.
[30] L. Liu, X. Li, S.H. Bo, Y. Wang, H.L. Chen, N. Twu, D. Wu, G. Ceder, High-performance P2-type $Na_{2/3}(Mn_{1/2}Fe_{1/4}Co_{1/4})O_2$ cathode material with superior rate capability for Na-ion batteries, Adv. Energy Mater. 5 (2015), 1500944.
[31] M. Sathiya, K. Hemalatha, K. Ramesha, J.M. Tarascon, A.S. Prakash, Synthesis, structure, and electrochemical properties of the layered sodium insertion cathode material: $NaNi_{1/3}Mn_{1/3}Co_{1/3}O_2$, Chem. Mater. 24 (2012) 1846–1853.
[32] S. Birgisson, T.L. Christiansen, B.B. Iversen, Exploration of phase compositions, crystal structures, and electrochemical properties of $Na_xFe_yMn_{1-y}O_2$ sodium ion battery materials, Chem. Mater. 30 (2018) 6636–6645.
[33] Y.J. Park, J.U. Choi, J.H. Jo, C.H. Jo, J. Kim, S.T. Myung, A new strategy to build a high-performance P′2-type cathode material through titanium doping for sodium-ion batteries, Adv. Funct. Mater. 29 (2019), 1901912.
[34] J.K. Park, G.G. Park, H.H. Kwak, S.T. Hong, J.W. Lee, Enhanced rate capability and cycle performance of titanium-substituted P2-type $Na_{0.67}Fe_{0.5}Mn_{0.5}O_2$ as a cathode for sodium-ion batteries, ACS Omega 3 (2018) 361–368.
[35] X. Sun, Y. Jin, C.-Y. Zhang, J.-W. Wen, Y. Shao, Y. Zang, C.-H. Chen, Na $[Ni_{0.4}Fe_{0.2}Mn_{0.4-x}Ti_x]O_2$: a cathode of high capacity and superior cyclability for Na-ion batteries, J. Mater. Chem. A 2 (2014) 17268–17271.
[36] X.H. Wu, J.H. Guo, D.W. Wang, G.M. Zhong, M.J. McDonald, Y. Yang, P2-type $Na_{0.66}Ni_{0.33-x}Zn_xMn_{0.67}O_2$ as new high-voltage cathode materials for sodium-ion batteries, J. Power Sources 281 (2015) 18–26.
[37] J. Xu, D.H. Lee, R.J. Clement, X.Q. Yu, M. Leskes, A.J. Pell, G. Pintacuda, X. Q. Yang, C.P. Grey, Y.S. Meng, Identifying the critical role of Li substitution in P2–$Na_x[Li_yNi_zMn_{1-y-z}]O_2$ ($0 < x,y,z < 1$) intercalation cathode materials for high-energy Na-ion batteries, Chem. Mater. 26 (2014) 1260–1269.
[38] Y. Wang, G. Hu, Z. Peng, Y. Cao, X. Lai, X. Qi, Z. Gan, W. Li, Z. Luo, K. Du, Influence of Li substitution on the structure and electrochemical performance of P2-type $Na_{0.67}Ni_{0.2}Fe_{0.15}Mn_{0.65}O_2$ cathode materials for sodium ion batteries, J. Power Sources 396 (2018) 639–647.
[39] S. Zheng, G. Zhong, M.J. McDonald, Z. Gong, R. Liu, W. Wen, C. Yang, Y. Yang, Exploring the working mechanism of Li^+ in O3-type $NaLi_{0.1}Ni_{0.35}Mn_{0.55}O_2$ cathode materials for rechargeable Na-ion batteries, J. Mater. Chem. A 4 (2016) 9054–9062.
[40] M. Bianchini, E. Gonzalo, N.E. Drewett, N. Ortiz-Vitoriano, J.M.L. del Amo, F. J. Bonilla, B. Acebedo, T. Rojo, Layered P2–O3 sodium-ion cathodes derived from earth abundant elements, J. Mater. Chem. A 6 (2018) 3552–3559.
[41] S.H. Guo, P. Liu, H.J. Yu, Y.B. Zhu, M.W. Chen, M. Ishida, H.S. Zhou, A layered P2- and O3-type composite as a high-energy cathode for rechargeable sodium-ion batteries, Angew. Chem. Int. Ed. Engl. 54 (2015) 5894–5899.
[42] Z.Y. Li, J.C. Zhang, R. Gao, H. Zhang, L.R. Zheng, Z.B. Hu, X.F. Liu, Li-substituted Co-free layered P2/O3 biphasic $Na_{0.67}Mn_{0.55}Ni_{0.25}Ti_{0.2-x}Li_xO_2$ as high-rate-capability cathode materials for sodium ion batteries, J. Phys. Chem. C 120 (2016) 9007–9016.
[43] J.H. Stansby, M. Avdeev, H.E.A. Brand, E. Gonzalo, N.E. Drewett, N. Ortiz-Vitoriano, N. Sharma, T. Rojo, Biphasic P2/O3-$Na_{2/3}Li_{0.18}Mn_{0.8}Fe_{0.2}O_2$: a structural investigation, Dalton Trans. 50 (2021) 1357–1365.

[44] M. Bianchini, E. Gonzalo, N.E. Drewett, N. Ortiz-Vitoriano, J.M. López del Amo, F. J. Bonilla, B. Acebedo, T. Rojo, Layered P2–O3 sodium-ion cathodes derived from earth abundant elements, J. Mater. Chem. A 6 (2018) 3552–3559.

[45] E. Lee, J. Lu, Y. Ren, X. Luo, X. Zhang, J. Wen, D. Miller, A. DeWahl, S. Hackney, B. Key, D. Kim, M.D. Slater, C.S. Johnson, Layered P2/O3 intergrowth cathode: toward high power Na-ion batteries, Adv. Energy Mater. 4 (2014), 1400458.

[46] S. Guo, P. Liu, H. Yu, Y. Zhu, M. Chen, M. Ishida, H. Zhou, A layered P2- and O3-type composite as a high-energy cathode for rechargeable sodium-ion batteries, Angew. Chem. Int. Ed. Engl. 54 (2015) 5894–5899.

[47] X. Qi, L. Liu, N. Song, F. Gao, K. Yang, Y. Lu, H. Yang, Y.S. Hu, Z.H. Cheng, L. Chen, Design and comparative study of O3/P2 hybrid structures for room temperature sodium-ion batteries, ACS Appl. Mater. Interfaces 9 (2017) 40215–40223.

[48] J. Chen, L.J. Li, L. Wu, Q. Yao, H.P. Yang, Z.S. Liu, L.F. Xia, Z.Y. Chen, J.F. Duan, S. K. Zhong, Enhanced cycle stability of $Na_{0.9}Ni_{0.45}Mn_{0.55}O_2$ through tailoring O3/P2 hybrid structures for sodium-ion batteries, J. Power Sources 406 (2018) 110–117.

[49] X. Rong, J. Liu, E. Hu, Y. Liu, Y. Wang, J. Wu, X. Yu, K. Page, Y.-S. Hu, W. Yang, H. Li, X.-Q. Yang, L. Chen, X. Huang, Structure-induced reversible anionic redox activity in Na layered oxide cathode, Joule 2 (2018) 125–140.

[50] B. Li, Y.Q. Wang, H.B. Rong, Y.T. Wang, J.S. Liu, L.D. Xing, M.Q. Xu, W.S. Li, A novel electrolyte with the ability to form a solid electrolyte interface on the anode and cathode of a $LiMn_2O_4$/graphite battery, J. Mater. Chem. A 1 (2013) 12954–12961.

[51] J.H. Li, L.P. Zhang, L. Yu, W.Z. Fan, Z.S. Wang, X.R. Yang, Y.L. Lin, L.D. Xing, M. Q. Xu, W.S. Li, Understanding interfacial properties between Li-rich layered oxide and electrolyte containing triethyl borate, J. Phys. Chem. C 120 (2016) 26899–26907.

[52] Y.M. Zhu, X.Y. Luo, M.Q. Xu, L.P. Zhang, L. Yu, W.Z. Fan, W.S. Li, J. Power, Failure mechanism of layered lithium-rich oxide/graphite cell and its solution by using electrolyte additive, J. Power Sources 317 (2016) 65–73.

[53] J.H. Li, L.D. Xing, L.P. Zhang, L. Yu, W.Z. Fan, M.Q. Xu, W.S. Li, Insight into self-discharge of layered lithium-rich oxide cathode in carbonate-based electrolytes with and without additive, J. Power Sources 324 (2016) 17–25.

[54] D. Eum, B. Kim, S.J. Kim, H. Park, J. Wu, S.-P. Cho, G. Yoon, M.H. Lee, S.-K. Jung, W. Yang, W.M. Seong, K. Ku, O. Tamwattana, S.K. Park, I. Hwang, K. Kang, Voltage decay and redox asymmetry mitigation by reversible cation migration in lithium-rich layered oxide electrodes, Nat. Mater. 19 (2020) 419–427.

[55] K. Dai, J. Wu, Z. Zhuo, Q. Li, S. Sallis, J. Mao, G. Ai, C. Sun, Z. Li, W.E. Gent, W. C. Chueh, Y.-D. Chuang, R. Zeng, Z.-X. Shen, F. Pan, S. Yan, L.F.J. Piper, Z. Hussain, G. Liu, W. Yang, High reversibility of lattice oxygen redox quantified by direct bulk probes of both anionic and cationic redox reactions, Joule 3 (2019) 518–541.

[56] J. Wu, Z. Zhuo, X. Rong, K. Dai, Z. Lebens-Higgins, S. Sallis, F. Pan, L.F.J. Piper, G. Liu, Y.-D. Chuang, Z. Hussain, Q. Li, R. Zeng, Z.-X. Shen, W. Yang, Sci. Adv. 6 (2020) eaaw3871.

[57] X. Cao, H.F. Li, Y. Qiao, M. Jia, X. Li, J. Cabana, H.S. Zhou, Adv. Mater. (2020), 2004280.

[58] Z.Y. Li, J.C. Zhang, R. Gao, H. Zhang, L.R. Zheng, Z.B. Hu, X.F. Liu, Li-substituted Co-free layered P2/O3 biphasic $Na_{0.67}Mn_{0.55}Ni_{0.25}Ti_{0.2-x}Li_xO_2$ as high-rate-capability cathode materials for sodium ion batteries, J. Phys. Chem. C 120 (2016) 9007–9016.

[59] R.R. Li, Y.Y. Liu, Z. Wang, J.L. Li, A P2/O3 biphasic cathode material with highly reversibility synthesized by Sn-substitution for Na-ion batteries, Electrochim. Acta 318 (2019) 14–22.

[60] K. Wang, Z.G. Wu, G. Melinte, Z.G. Yang, A. Sarkar, W.B. Hua, X.K. Mu, Z.W. Yin, J.T. Li, X.D. Guo, B.H. Zhong, C. Kübel, Preparation of intergrown P/O-type biphasic layered oxides as high-performance cathodes for sodium ion batteries, J. Mater. Chem. A 9 (2021) 13151–13160.

[61] N.P.W. Pieczonka, Z.Y. Liu, P. Lu, K.L. Olson, J. Moote, B.R. Powell, J.H. Kim, Understanding transition-metal dissolution behavior in $LiNi_{0.5}Mn_{1.5}O_4$ high-voltage spinel for lithium ion batteries, J. Phys. Chem. C 117 (2013) 15947–15957.

[62] R. Jung, F. Linsenmann, R. Thomas, J. Wandt, S. Solchenbach, F. Maglia, C. Stinner, M. Tromp, H.A. Gasteiger, Nickel, manganese, and cobalt dissolution from Ni-rich NMC and their effects on NMC622-graphite cells, J. Electrochem. Soc. 166 (2019) A378–A389.

[63] C. Zhan, T.P. Wu, J. Lu, K. Amine, Dissolution, migration, and deposition of transition metal ions in Li-ion batteries exemplified by Mn-based cathodes – a critical review, Energy Environ. Sci. 11 (2018) 243–257.

[64] Z. Zhu, H. Peelaers, C.G. Van de Walle, Hydrogen-induced degradation of $NaMnO_2$, Chem. Mater. 31 (2019) 5224–5228.

Cong Chen is currently pursuing his M.Sc. degree under the supervision of Prof. Feng Pan at Peking University Shenzhen Graduate School, China. He received his B.Eng. from South China University of China in 2018. His research interests mainly concentrate on the relationship between structure and property, and modifying strategies of Na iron anode material.

Weiyuan Huang received his B.S. degree from South China Normal University in 2017. He is pursuing his Ph.D. degree in the School of Advanced Materials, Peking University, China. His research interests mainly focus on cathode materials for lithium ion batteries and sodium ion batteries, especially on layered oxide materials including Mn-rich layered oxides and high voltage $LiCoO_2$ layered oxides.

Yiwei Li received his B.S. degree in College of Materials science and Engineering from Huazhong University of science and technology in 2017. He is currently a Ph.D. candidate in School of Advanced Materials at Peking University. His main research work is Li-Rich cathode materials with high voltage and high energy density for Li ion batteries.

Mingjian Zhang is currently an associate research professor in School of Advanced Materials, Peking University. He got his Ph.D. degree from Fujian Institute of Research on the Structure of Matter, Chinese Academy of Sciences in 2013, then worked there as an assistant research fellow for one year. He was a research scholar in Brookhaven National Lab from 2016 to 2019, then in the University of Chicago in 2019. He mainly works on high-performance cathodes for Li-ion batteries, especially the structural evolution and structure-property research of the cathodes.

Kaiqi Nie is currently an assistant research fellow at the Institute of High Energy Physics, Chinese Academy of Sciences, China. She received her Ph.D. degree in material science at the Institute of Functional Nano & Soft Materials (FUNSOM) at Soochow University in 2018, and then she performed post-doctoral research at the Helmholtz-Zentrum Berlin für Materialien und Energie GmbH from 2018 to 2020. Her research interests focus on the investigation of energy materials by using synchrotron-based X-ray spectroscopy.

Jiaou Wang is an associate research fellow at Institute of High Energy Physics, Chinese Academy of Sciences, China. He received his Ph.D. degree in Condensed Matter Physics and graduated from Lanzhou University (2009). From 2009 to now, he has been working at 4B9B beamline of Beijing Synchrotron Radiation Facility in IHEP. His current research interests focus on the Methodology of Synchrotron radiation.

Wenguang Zhao is an engineer in the School of Advanced Materials, Peking University Shenzhen Graduate School, China. He has over 10 years' experience in material characterization using wide range of analytical tools including XRD, XPS, SEM and TEM. His research interests mainly focus on the Ex/in-situ TEM and Ex/in-situ XRD characterization of battery materials.

Rui Qi is currently pursuing his M.Sc. degree under the supervision of Prof. Feng Pan at Peking University Shenzhen Graduate School, China. He received his B.Eng. from Central South University in 2018. His research interests mainly focus on investigating the relation between the structure of cathode materials for Li- and Na-ion batteries and their electrochemical behavior.

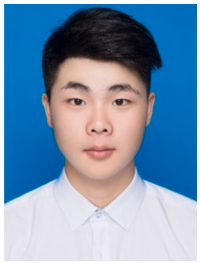

Changjian Zuo is currently pursuing his M.Sc. degree under the supervision of Prof. Feng Pan at Peking University Shenzhen Graduate School, China. He graduated from Soochow university and received his B. S. degree from the School of Shangang Iron and Steel in 2018. His research interests focus on the cathode materials of lithium ion batteries.

Zhibo Li received his B.S. degree from South China Normal University in 2018. He is currently a M. S. student under the supervision of Prof. Feng Pan at the school of Advanced Material, Peking University. His research interests mainly focus on layered cathode material for lithium ion batteries.

Haocong Yi received his B.S. degree from Huazhong University of Science and Technology (HUST, China) in 2018. He is currently a Ph.D. degree candidate under the supervision of Prof. Feng Pan in School of Advanced Materials, Peking University Shenzhen Graduate School, China. His research interests focus on the lithium ion batteries.

Feng Pan, founding Dean of School of Advanced Materials, Peking University Shenzhen Graduate School, got B.S. from Dept. Chemistry, Peking University in 1985 and Ph.D. from Dept. of P&A Chemistry, University of Strathclyde, Glasgow, UK, with "Patrick D. Ritchie Prize" for the best Ph.D. in 1994. With more than a decade experience in large international incorporations, Prof. Pan has been engaged in fundamental research and product development of novel optoelectronic and energy storage materials and devices. As Chief Scientist, Prof. Pan led eight entities in Shenzhen to win 150 million RMB grant for the national new energy vehicles (power battery) innovation project since 2013.